J. Fluid Mech. (1971), *vol.* 50, *part* 3, *pp.* 493–512
Printed in Great Britain

Spatial structure in the viscous sublayer

By A. K. GUPTA, J. LAUFER AND R. E. KAPLAN
Department of Aerospace Engineering,
University of Southern California, Los Angeles

(Received 17 February 1971 and in revised form 25 June 1971)

An experimental investigation was performed to study the spatial coherence of structures in the sublayer of a turbulent boundary layer observed previously by flow visualization. The present work verifies these observations in an Eulerian reference frame and develops a statistical description of the phenomenon. The technique involves simultaneous digital sampling of an array of constant temperature hot-wire anemometers arranged to extract information about a spanwise variation in flow quantities. The quantitative description agrees with dimensionless measures of the structure scales previously published.

1. Introduction

Experimental turbulence research of the past thirty years has relied heavily on the Reynolds formulation of the governing equations. Indeed, the mean momentum and turbulent kinetic energy equations provide a convenient way of describing the force and energy balances realized over a sufficiently long period of time in the flow field. The higher order terms arising in these equations, as a result of the Reynolds formulation, have been considered the key to the understanding of the turbulence problem and it was only natural that a considerable portion of the experimental effort concentrated on the measurement of these quantities. There is no question that such work has been useful and that new information has been obtained by such experiments. However, many researchers in this field now realize that although modern techniques enable the measurement of any desired higher order correlations these are not likely to lead to a direct understanding of the problem. In order to make any progress in understanding this difficult question a different approach is necessary.

In the Reynolds formulation the various flow quantities are split, in a rather arbitrary fashion, into a temporal mean and a time-dependent part. Furthermore the mean values in the governing equations are taken over a sufficiently long averaging time. There seems to be considerable concern that significant information is lost in this 'long-time' averaging process, information that might aid in the understanding of the problem. In fact, one piece of evidence that gives more than sufficient support to such concern has already been uncovered; namely, the discovery of the laminar turbulent interface in free turbulent shear layers by Corrsin (1947) which is believed to be one of the major accomplishments of experimental research in turbulence. The subsequent work of Townsend (1956) on the entrainment process and the large-scale equilibrium hypothesis is critically

dependent on the existence of such an interface. It is to be noted, however, that the discovery was not motivated by any theoretical considerations. In fact at this point it is not even clear whether the dynamics of the interface motion can be treated using a Reynolds type of formulation.

It was only natural that some experimenters abandoned the use of existing theoretical formulations as guide-lines for developing ideas for their experimental programs. Instead, they recoursed to visual observations and, using modern optical and computational techniques, were able to produce new and interesting results. Particular reference is made here to some studies of the viscous sublayer by Hama (Corrsin 1957) who noted a characteristically streaky behaviour of the flow, by Bakewell & Lumley (1967), by Corino & Brodkey (1969) and in particular by the Stanford group in a series of papers starting with Kline & Runstadler (1959) and, more recently, Kline *et al.* (1967). They have discovered a more or less deterministic coherent structure in the sublayer, occurring randomly in space and time, the existence of which was shown to very probably have a bearing on the turbulence production mechanism.

More recently three other papers have come to our attention on closely related areas, Rao, Narasimha & Narayanan (1971), Kim, Kline & Reynolds (1971), and Grass (1971).

The present work was strongly motivated by these results. The main goal in formulating and programming the experiments was to see whether or not, with the simultaneous use of a number of hot wires, it would be possible to obtain a more quantitative picture of the flow conditions existing in the viscous sublayer. Early in the investigation it became apparent that the use of a conventional long-time averaging process in obtaining certain statistical quantities did not reveal any structure referred to above. It was conjectured that this randomly occurring structure has a relatively short lifetime and, consequently, an averaging process that provides the possibility of revealing such a structure, if it indeed exists, and at the same time has a statistically meaningful definition, had to be developed. Considerable time and effort has been spent in developing such a technique and although the method reported in this paper is not yet considered general enough it served the main purpose of this work.

2. Experimental equipment

2.1. *Wind tunnel*

Experiments covering a speed range from 11 to 40 ft/sec and Reynolds number based on momentum thickness from 2000 to 6500 were carried out in the USC low-speed low turbulence wind tunnel. This is an open-circuit continuously variable speed tunnel with a contraction ratio of $16\frac{1}{2}$, a rectangular test section of 3×2 ft, and a streamwise fluctuation turbulence level of 0·28 %. The general layout of the tunnel is sketched in figure 1. In order to fix the location of transition, the working surface and side-wall boundary layers were tripped about 15·5 ft upstream from the test station, and the flow entered the fan about 9 ft downstream from the station.

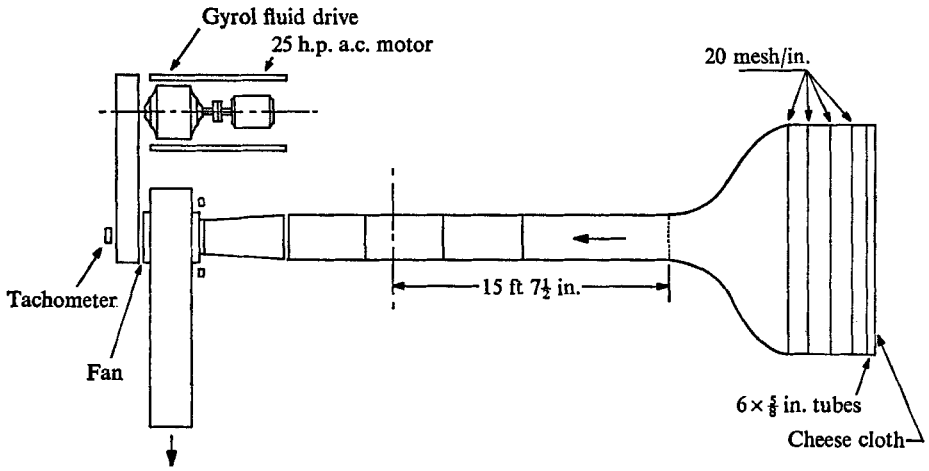

FIGURE 1. USC 3 × 2 ft low turbulence wind tunnel.

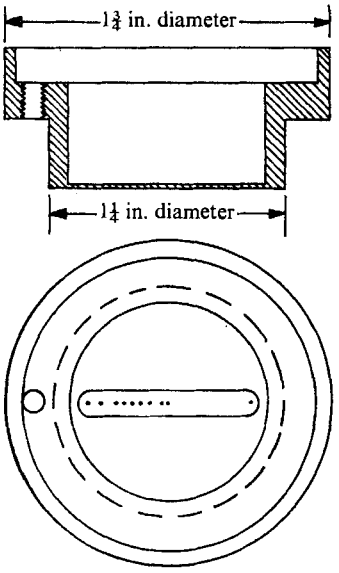

Wire pair	10, 9	10, 8	10, 7	10, 6	10, 5	10, 4	10,3	10, 1	10, 2
Spacing (in.)	0·021	0·077	0·126	0·182	0·222	0·275	0·341	0·42	−0·38

FIGURE 2. Front and plan views of u plug.

2.2. *The plug probe*

The hot wires were mounted on a Plexiglas plug with the surface exposed to the flow flush with the wall. The elevation of all but one wire was 0·014 in. At the two extreme free-stream velocities of 11·3 ft/sec and 39·5 ft/sec, nine of the ten wires spanned a dimensionless distance of 101 and 324 respectively, (in sublayer co-ordinates) corresponding to a fixed span of 0.42 in. The dimensionless elevation, yu^*/ν, was less than 12 at all wind speeds. Briefly, the construction of the plug probe can be described as follows: the plug (figure 2) was machined out of a Plexiglas block and series of 0·004 in. holes were drilled with positional accuracy of 0·001 in. in a milled slot in the plug. Tinned jeweller's brooches with a tip diameter of 0·003 in. were then inserted in the holes and the elevation of their tips fixed by placing a 0·014 in. feeler gauge between the plug surface and a flat table. The slot in the plug was then filled with epoxy cement. Next the ends of the brooches inside the plug were soft-soldered to electrical lead wires. Finally, the rear surface of the plug was covered with a cap. Thus the plug in its finished form had prongs for hot wires on one end and the electrical plug-in leads for an equal number of hot wires on the opposite end. An enlarged picture of this probe is shown in figure 3 (plate 1).

Except for a few cases platinum wire of diameter 5×10^{-5} in. was used as hot wire. With a length of 0·014 in. the aspect ratio of the wires was 280. The choice of 0·014 in. wire elevation was dictated by the requirement that the wires be within the viscous sublayer at all usable wind speeds.

The wires on the probe were spaced so that the distance between adjacent wire pairs was non-uniform which yielded a more uniform distribution of separation between arbitrary wire pairs. The one isolated wire was included with the objective of obtaining conventional correlations for larger lateral distances. The second wire from the left (figure 3) was mounted flush with the wall to observe the wall shear fluctuations. In the early stages of data analysis attempts were made to use this signal as a detector function for computing short-time conditional correlations, but no significant success was achieved by its use.

The plug was inserted into a hole cut out of the upper Plexiglas wall of the tunnel along its centre-line. When the plug probe was not being used another flat-ended Plexiglas plug covered the hole. The surface discontinuities formed by the circular edges of the plugs with the tunnel wall surface were measured by a dial-gauge. The leading edge of the flattened plug formed a cavity of depth 5×10^{-4} in., while that of the plug probe formed a step of height 15×10^{-4} in., small compared to typical sublayer dimensions.

2.3. *The hot-wire anemometer and amplifier set*

Constant-temperature hot-wire anemometers with frequency response flat over the range d.c.–30 kHz were used. Up to 14 of these sets could be operated simultaneously with a common power source of ± 15 V. Output of each hot-wire set entered an isolation amplifier which also subtracted a fixed voltage from the hot-wire bridge output and amplified the difference by a factor of ten for tape recording. The signal-to-noise ratio for the combined hot-wire

anemometer, amplifier and tape recorder's record amplifier was 70 db (Kaplan & Laufer 1969).

By selecting the resistor in one of the four arms of the hot-wire bridge appropriately, the overheat ratio (hot resistance/cold resistance) for the hot wires was kept at 1·33. This low overheat ratio was chosen in order to minimize the free-convection effects in the low-speed region near the wall and to minimize the conduction effects of a heated wire near a solid wall. According to the formula given by Collis & Williams (1959) the free-convection limit for the present case was approximately 0·1 ft/sec. The effect of the wall vicinity is the same for all wires and has been discounted in subsequent analysis.

2.4. *Tape recorder and other equipment*

A Hewlett–Packard model 3955A, fourteen channel F.M. magnetic tape recording system was used for recording the outputs of the anemometers. The recording speed for all data was 60 in./sec and the tapes were played back for digitizing at speeds of either 15 in./sec or $1\frac{7}{8}$ in./sec. The effective bandwidth was d.c.–20 kHz, while the total signal-to-noise ratio was improved as described above by maintaining in excess of 40 db S/N of fluctuations.

The other equipment used at different stages of the experiments was the following: a pitot tube of hole diameter 0·03 in. together with a mks Baratron pressure meter with 3 mm Hg pressure sensor to obtain mean velocity profiles; a 2 in. micrometer screw traverse; a modified integrating digital voltmeter (Non-linear Systems 2914) to average d.c. voltages over ten or twenty seconds; a Hewlett–Packard 132*a* dual beam oscilloscope to monitor the signals; a Hewlett–Packard root mean square voltmeter; a General Radio 2*c*–2*Mc* oscillator; an ASTM bomb calorimeter thermometer with a resolution of 0·02 °C. Care was taken throughout to minimize possible errors in data acquisition.

3. Experimental procedure

The experimental and computing techniques were basically similar to those described by Kaplan & Laufer (1969). Briefly stated, the data for each reading were recorded for 50 seconds on as many channels of the tape recorder as the number of hot wires in use. For instance, with the plug probe in operation the signals, one from each hot wire, were stored in ten adjacent channels of the tape. At the same time, the average input and output voltages to each bucking voltage amplifier were noted together with the wind speed and the temperature in the tunnel.

The analog tape was then played back at a slower speed for digitizing a sample length corresponding to 10 sec of real time. This digitized turbulence signal was stored on a single magnetic disk cartridge (IBM 2315) for subsequent computations. The higher wind-speed signals were digitized at a faster rate in order to retain their high frequency components.

The analog to digital converters generated a thirteen bit binary number with a fourteenth sign bit with respect to ± 10 V full scale resulting in a resolution of approximately 1·2 mV. Since the sublayer was the region of high a.c. level and also the record voltages were an order of magnitude less than the bucking voltage, the signal-to-noise ratio at playback exceeded 56 db.

Prior to running the systematic set of experiments, characteristics of the turbulent boundary layer such as the mean velocity profile and r.m.s. fluctuation level were established. These showed that the flow near the working station was weakly accelerating, $(2\theta/\rho U_0^2)dp/dx = -0{\cdot}8 \times 10^{-3}$. Spanwise variation of the mean flow was negligible over one plug diameter span as illustrated in figure 4(*a*) and (*b*), where the mean velocities and the r.m.s. of fluctuations are plotted. It is seen that the scatter is within the accuracy of the measurements: less than $\pm 1{\cdot}0$ per cent for the mean velocity ($\bar{U}/U_0$) at the two typical wind speeds of 11·3 ft/sec and 39·5 ft/sec and less than $\pm 5{\cdot}0$ per cent for the r.m.s. fluctuations. The mean velocity and the r.m.s. fluctuation profiles across the turbulent boundary layer were in good agreement with past measurements.

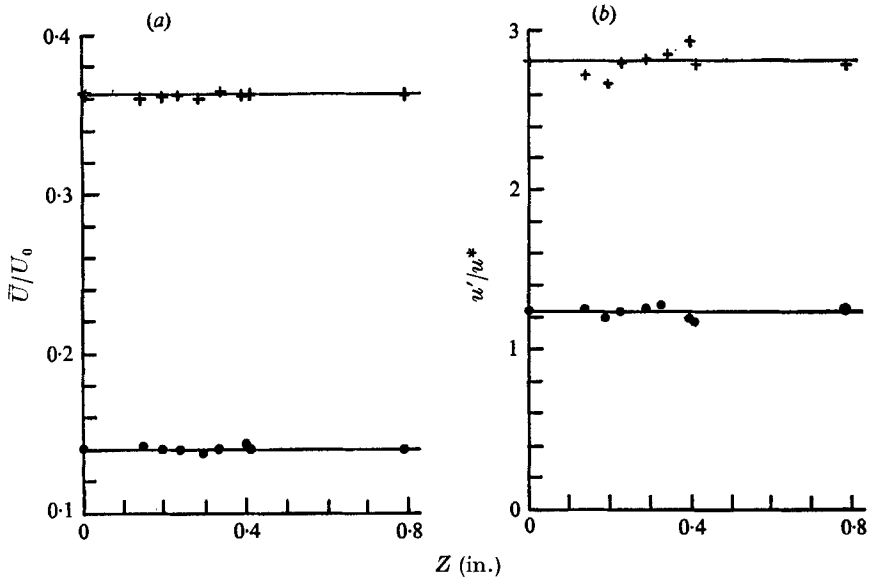

FIGURE 4. Two-dimensionality of flow over u plug probe. ●, $U_0 = 11{\cdot}3$ ft/sec; $\bar{U} = 1{\cdot}57$ ft/sec; $u^* = 0{\cdot}46$ ft/sec; +, $U_0 = 39{\cdot}5$ ft/sec; $\bar{U} = 14{\cdot}46$ ft/sec; $u^* = 1{\cdot}48$ ft/sec.

3.1. *Calibration*

For the calibration of hot wires on the plug probe it was assumed that the y position of the wires was known. An examination of the y positions of the wires with a microscope fitted with a graduated eye piece (0·0005 in. spaced graduations) showed this to be reasonable. Thus, with the free-stream velocity U_0 known, the local velocity at wire locations was determined from the following relations:

$$\delta(x) = 0{\cdot}37(U_0 x/\nu)^{\frac{1}{5}},$$

$$U_0/u^* = 2{\cdot}51 \ln(\delta u^*/\nu) + 7{\cdot}38,$$

where ν, the kinematic viscosity of air, was 160×10^{-6} ft^2/sec, $x = 12{\cdot}51$ ft, δ the boundary-layer thickness and u^* the friction velocity. The second relation above is Clauser's (1956) matching velocity profile. These two equations were solved numerically to obtain friction velocity u^* up to three decimal places. The linear law of the wall relation was then used to find the local velocity $\bar{U}$ for $y^* \leqslant 7$. For

$y^* > 7$ the local velocity was determined graphically from the known mean velocity profile.

Thus, for each wire the mean voltage outputs E as a function of varying local mean speed $\overline{U}$ were noted. Calibration constants A and B in King's law,

$$E^2 = A + B(\overline{U})^{\frac{1}{2}},$$

were obtained by the method of least squares. Near the zero velocity ordinate secondary fits for each calibration curve were approximated by two straight lines of increasing slope (in the E^2, $(\overline{U})^{\frac{1}{2}}$ plane), which merged with the main calibration curve. Thus there were two discontinuities in the slope of a calibration curve at points where first and second, and second and third (or main) calibration lines intersected. This was considered a workable approximation to the free-convection limit of the calibration curves for the fixed elevation wires.

3.2. *Computing method*

The main programs were written in FORTRAN IV and were run on an IBM computer model 360/44 (16000 Word Memory). The tasks performed were data acquisition, calibration, and calculation.

Data acquisition. Under control of an external clock, Analog-Digital conversions were initiated and temporarily stored on the disk. This program could handle a 10 sequential channel ADC request at an interval of 480 μsec, limited by the disk rotational delay. Total capacity of the disk exceeded 500000 conversions.

Calibration. During a subsequent run the data were retrieved from the disk. It was calibrated in two stages. First, the raw digital data from the converters were transformed from 16 bit integer numbers to 32 bit floating-point voltages, using the properties of the converters and average measurements made at recording time. Then these voltages were converted to velocities, again using the calibration for each wire measured at recording time. This scheme was considered adequate for this experiment.

Variable interval time averaging (VITA) process. For a conventionally defined average quantity of a stationary random function, say

$$\bar{Q}(x_i) \equiv \frac{1}{T}\int_{t_0}^{t_0+T} Q(x_i, t)\,dt,$$

the time interval T has to be chosen large enough, by experiment, to ensure that $\bar{Q}$ becomes independent of T. However, if the function $Q(x_i, t)$ were to contain certain information that has a short lifetime compared to T, such information would be smeared out or possibly lost in $\bar{Q}$. One statistical method that enables one to study this problem is the variable interval time averaging (VITA) process. We define

$$\hat{Q}(x_i, t_0; T_s) = \frac{1}{T_s}\int_{t_0}^{t_0+T_s} Q(x_i, t)dt.$$

In general $\hat{Q}$ is a random function of t_0. By observing the behaviour of $\hat{Q}$ in the present experiments it was possible to extract certain statistical features discussed in the next section.

In particular, the correlation function $\hat{R}_{uu}(0, 0, Z, t_0; T_s)$ using the VITA process was computed as follows. Let $1/\tau$ be the sampling rate, $U_t(z)$ be the instantaneous value of the velocity sample and N be the total number of samples taken during the averaging period T_s. Then $T_s = N\tau$ and

$$\hat{R}_{uu}(0, 0, Z, t_0; T_s) = \frac{\frac{1}{N}\sum_1^N [U_t(z) - \tilde{U}][U_t(z+Z) - \tilde{U}]}{\left\{\frac{1}{N}\sum_1^N [U_t(z) - \tilde{U}]^2 \times \frac{1}{N}\sum_1^N [U_t(z+Z) - \tilde{U}]^2\right\}^{\frac{1}{2}}},$$

the first sample being taken at $t = t_0 + \tau$ and the nth sample at $t = t_0 + n\tau$.

Various definitions of $\tilde{U}$ were tried including the VITA of U_t at each station z, the average of the VITA's for all stations and the long-time average. The first choice shows the departures from the observed structures during the averaging time, the second gives the departures from the instantaneously observed spatial average while the last has too little resolution to be of use. The first scheme was adopted in presenting the data although the second scheme lead one to essentially the same conclusions.

3.3. *Source of error*

While the data acquisition system design tended to minimize most sources of instrument error one unavoidable source remained. Since voltage averages in the wind tunnel were made over 10 sec in the tunnel it was not possible to measure them coincidentally with the recording. Hence, averages measured on the computer do not in general correspond to those measured in the laboratory. This minor calibration problem appeared noticably only when the record voltage fell below 100 mV, and is not reflected in the measurements presented here.

It should be noted that the calibration technique is significantly different from that described in Kaplan & Laufer (1969) in which these problems did not occur.

The digital accuracy in data processing carried many more significant bits than existed in the data, and within the framework of the VITA, introduced no errors.

4. Results and discussion

4.1. *Nature of the velocity correlations measured by VITA*

It became evident in the early stages of the experimental program that the conventional spatial correlation function $R_{uu}(0, 0, Z)$ is not the relevant quantity to measure if one seeks to detect and identify the 'streaky' nature of the viscous sublayer, as discussed in the introduction. Indeed, figure 5 shows a number of R_{uu} distributions obtained at various Reynolds numbers and none of them exhibit features that would suggest the existence of any spatial structure. The slight waviness observed in the distributions corresponding to the lower Reynolds numbers is too small in amplitude for one to attempt to attach any significance to it.

In contrast, the reader is referred to figure 6 which contains a number of correlation functions $\hat{R}_{uu}$ measured with the VITA technique at $U_0 = 18{\cdot}8$ ft/sec. The

maximum separation distance is 0·42 in. or in this case about 16 sublayer thicknesses ($Z^* = 163$). The averaging period varied between $\frac{3}{8}$ msec to 6·75 sec. The starting time for the averaging (t_0) and the sampling rate (8 kHz) were the same for all the traces.

There are several qualitative observations one can immediately make from this figure. (i) Perhaps the most startling features are the strong positive and negative correlations occurring over many sublayer thicknesses apart, suggesting

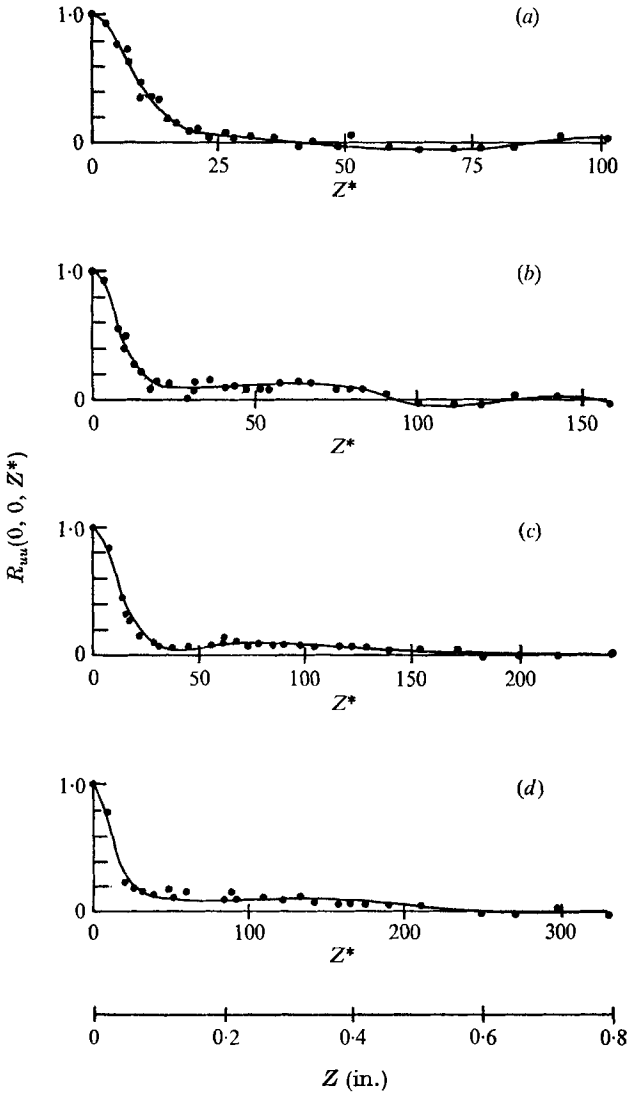

FIGURE 5. Two-point spanwise correlation of u fluctuations. $R_{uu}(0, 0, Z)$ at various velocities. $y = 0{\cdot}014$ in.

	(*a*)	(*b*)	(*c*)	(*d*)
R_θ ($\simeq$)	2200	3300	4700	6500
U_0 (ft/sec)	11·3	18·8	20·0	39·5
y^*	3·4	5·4	7·8	10·8

the presence of a spatial structure. (ii) As the averaging period T_s is increased the high correlations diminish, in fact for $T_s = 6{\cdot}75$ sec they are smeared out completely and the correlation function has essentially the same shape as the conventional long-time averaged one (see figure 5). (iii) If one is to study the lateral structure that presumably produces the high correlations the averaging times have to be kept relatively short.

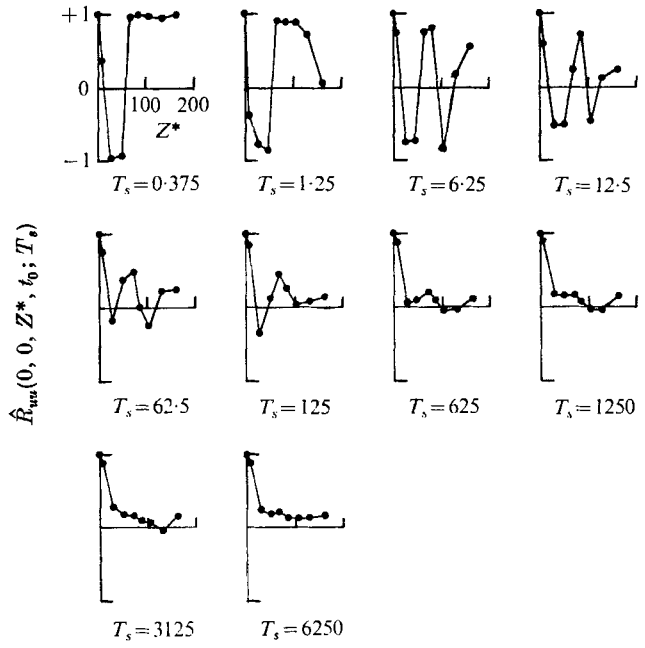

FIGURE 6. Two-point correlation $\hat{R}_{uu}(0, 0, Z^*, t_0; T_s)$ as a function of averaging time (msec) T_s, computed by the VITA process. $R_\theta \simeq 3300$, $U_0 = 18{\cdot}8$ ft/sec, $y^* = 5{\cdot}4$.

4.2. *The spanwise structure*

Before speculating any further about the existence and nature of the structure it is instructive to observe a number of correlation functions obtained by the VITA technique. Figures 7 and 8 each show ten such distributions measured sequentially; that is, t_0 of the nth distribution is equal to $(t_{0n-1} + T_s)$ where the averaging time is kept constant in each figure (0·375 and 1·25 msec).

It is to be noted that the strong correlations over large distances (relative to the sublayer thickness) are again present for each case and that qualitatively speaking certain shapes of the correlation function occur more often than others. For instance, distribution figures 7 (*b*), (*c*), (*d*), (*f*), (*j*), and 8 (*c*), (*d*), (*f*), (*h*) all seem to have similar shapes suggesting a spatially periodic flow field across the wire array with a wavelength of between 0·2 and 0·4 in. ($75\,\nu/u^* < \lambda < 150\,\nu/u^*$). Referring back to figure 6, it is seen that this wavelength is still detectable for averaging times as long as a second ($T_s \sim 70\,\delta/U_0$) although the magnitude of the correlations has decreased considerably.

The problem one is faced with may be now stated as follows. Is it possible to extract from the type of correlation distributions described above a statistically meaningful quantity which would provide proof of the existence of a spatial structure?

In the early stages of the analysis an attempt was made to devise a conditional sampling technique with which a statistically definable correlation function could be obtained. It was conjectured that the similar periodic distributions described previously appear at times when particular events occur at or near the wall. According to the observations of Kline *et al.* (1967), the occurrence of the periodic structure is usually preceded by a local reversal in sign of the velocity gradient and, in turn, a large change in the instantaneous value of the local skin friction. Thus, using a hot wire placed on the insulated wall as a skin friction indicator, computations of short-time correlations may be initiated at instances when the wall wire indicates extreme values of the skin friction. However, no improvement in the method of obtaining a quasi-stationary form of the correlation function has been achieved with this technique. Sufficient effort has not been made at this time to decide whether the lack of correlation lies in the physics of the problem or the technique.

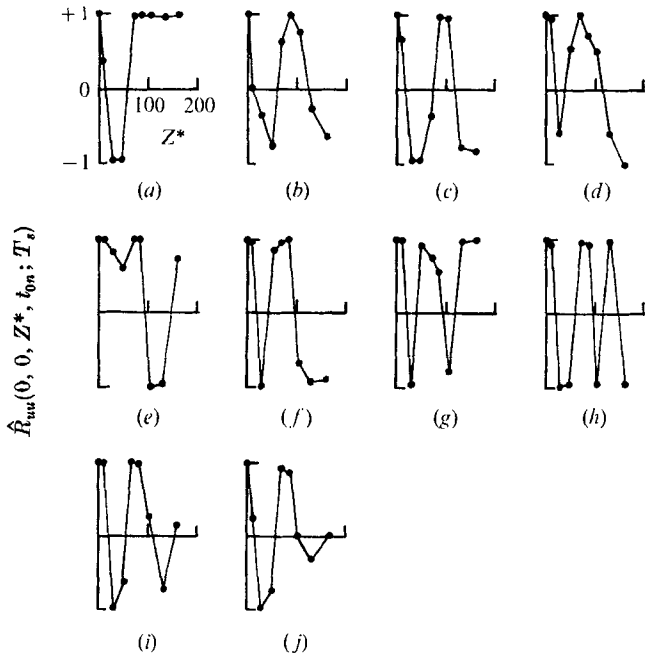

FIGURE 7. Typical two-point correlations $\hat{R}_{uu}$ (0, 0, Z^*, t_{0n}; T_s) with T_s = 0·375 msec, $R_\theta \simeq$ 3300, U_0 = 18·8 ft/sec, y^* = 5·4.

For the purpose of the present study, it was felt, that the measurement of a statistically meaningful wavelength would be sufficient indication of the existence of a spatially periodic structure. To this end the following method was initially adopted. For one free-stream velocity, U_0, N short-time correlations were

computed for a fixed value of averaging time T_s. These functions are denoted by $\hat{R}_{uu}(0, 0, Z, t_{0n}; T_s)$, where n is an integer between 1 and N; from this function the location of the first minimum $Z_{\min}$ and the first maximum $Z_{\max}$ are found. By letting the integer α_i be the number of times the first maximum occurs at Z_i a frequency polygon for $Z_{\max}$ is made. The mean values of the maxima locations and their standard deviation σ can then be calculated as follows.

$$\bar{Z}_{\max} = \Sigma Z_{i(\max)}\alpha_i / \Sigma\alpha_i,$$

$$\sigma^2 = \Sigma(Z_{i(\max)} - \bar{Z}_{\max})^2 \alpha_i / \Sigma\alpha_i,$$

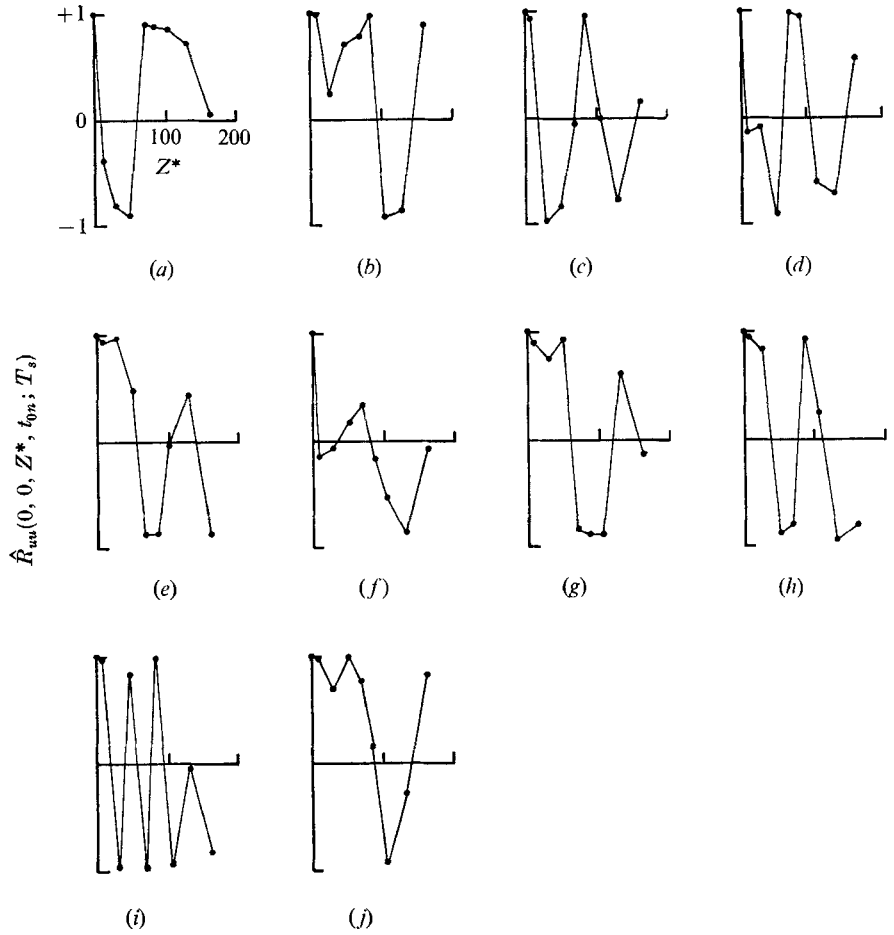

FIGURE 8. Typical two-point correlations $\hat{R}_{uu}$ $(0, 0, Z^*, t_{0n}; T_s)$ with $T_s = 0{\cdot}375$ msec, $R_\theta \simeq 3300$, $U_0 = 18{\cdot}8$ ft/sec, $y^* = 5{\cdot}4$.

where $\Sigma\alpha_i = N$. Replacing $Z_{i(\max)}$ by $Z_{i(\min)}$ in the above expressions, the location of the mean value of the minima and their standard deviations can initially be determined. It is conjectured that if a mean value can so be determined in a consistent fashion, that is, independently from T_s (within some set limits), then the existence of a periodic structure with a mean wavelength $\lambda \simeq \bar{Z}_{\max}$ can be

considered to be established. It follows that $\bar{Z}_{\min}$ would then correspond approximately to the half wavelength.

Thus, for a fixed value of the averaging time T_s a pair of frequency polygons determines the location of the mean values of the full and half wavelengths. By varying the value of T_s, sample mean values and standard deviation as a function of the averaging time were obtained. A typical set of results so obtained, corresponding to a wind speed of $U_0 = 18{\cdot}81$ ft/sec, is presented in figures 9–11.

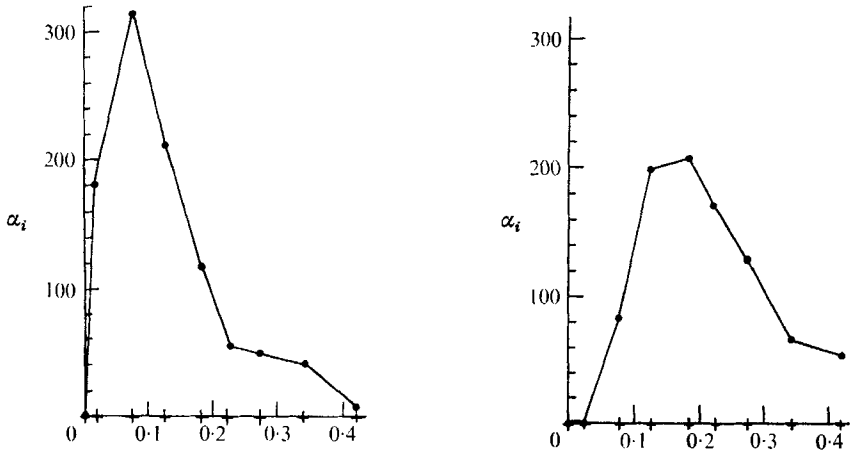

FIGURE 9. Frequency polygons for the occurrence of the first maxima $Z_{i(\max)}$ and the first minima $Z_{i(\min)}$ of the correlations $\hat{R}_{uu}$ (0, 0, Z, t_{0n}; T_s). $U_0 = 18{\cdot}8$ ft/sec, $T_s = 0{\cdot}375$ msec, $s = 3$, $\Sigma\alpha_i = 1000$, $\sigma = 0{\cdot}11$ in.

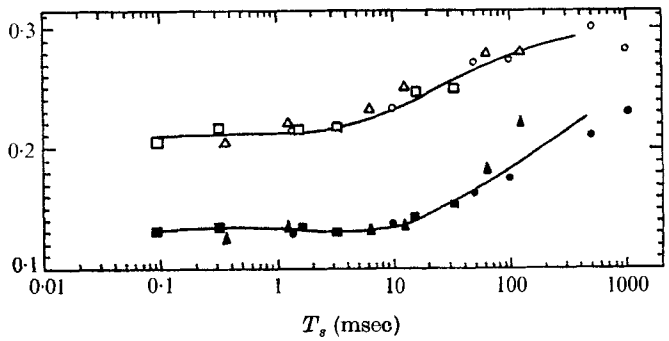

FIGURE 10. $\bar{Z}_{\max}$ and $\bar{Z}_{\min}$ of the correlations $\hat{R}_{uu}$ (0, 0, Z, t_{0n}; T_s) as a function of averaging time T_s. $U_0 = 18{\cdot}8$ ft/sec, $R_\theta \simeq 3300$. □, 32 kHz; △, 8 kHz; ○, 2 kHz. Open symbols, maximum; dark symbols, minimum.

Figure 9 shows two frequency polygons corresponding to $T_s = 0{\cdot}375$ msec. The crosses on the abscissa indicate the location of hot wires on the plug probe. The total number of correlations N from which these frequency polygons are made is 1000. The mean values and their standard deviations, obtained in the manner described above from these frequency polygons, are also indicated. It is important

to note that the frequency polygon corresponding to $Z_{i(\max)}$ does not close completely and that $\bar{Z}_{\max}$ is not exactly twice $\bar{Z}_{\min}$ as expected. This indicates a limitation of the fixed geometry probe causing a small but meaningful error in the corresponding results, to be more fully discussed in a subsequent section. The variation of the magnitude of $\bar{Z}_{\min}$ and $\bar{Z}_{\max}$ as a function of the averaging time T_s and the variation of the corresponding standard deviations is shown in figure 10. Three sets of points for each curve represent digitizing rates of 2, 8 and 32 kHz thus effectively covering a wide range of T_s. It is seen from figure 10 that below a certain value of the averaging time, $T_s \simeq 3$ to 10 msec in the present case, $\bar{Z}_{\max}$ and $\bar{Z}_{\min}$ become independent of T_s.

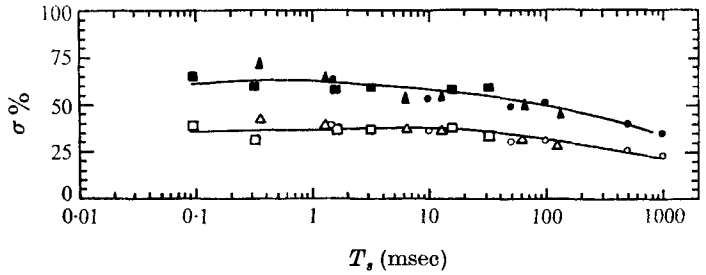

FIGURE 11. Percentage standard deviation of $Z_{\max}$ and $Z_{\min}$ as a function of averaging time T_s. $U_0 = 18{\cdot}8$ ft/sec, $R_\theta \simeq 3300$. □, 32 kHz; △, 8 kHz; ○, 2 kHz. Open symbols, maximum; dark symbols, minimum.

This result is gratifying since it gives one confidence in the consistency of the method adopted and provides a basis for accepting the existence of a statistically meaningful wavelength. Its absolute value, however, is still to be determined. Also the significance of the upper limit for the averaging time will be discussed subsequently.

If the statistically determined wavelength described above is indeed a characteristic parameter of a spatial structure, as conjectured, one would expect it to vary, say, with the free-stream velocity and to scale with preferably a single boundary-layer length parameter. Figure 12 shows that as the free-stream velocity is changed the position for the highest values of α_i/N shifts as expected. The figure also reveals a difficulty already referred to previously that is inherent in the use of a fixed hot-wire rake. If the wavelength to be determined is larger than or nearly equal to the maximum wire separation (0·42 in. in this case) the probability distribution curve does not close and the determination of the mean values. $\bar{Z}_{\max}$ becomes problematical. On the other hand for small wavelengths (say $\lambda < 0{\cdot}2$ in.) the spatial resolution of the probe raises obvious difficulties. For instance, the first *detected* maximum cannot appear until the *third* wire. These circumstances impose definite limitations on the Reynolds number range of the experiments within which the scaling laws can be quantitatively investigated. Figure 13 shows a number of frequency polygons obtained for four Reynolds numbers. The points cover the complete range of averaging periods for which the calculated wavelength is independent of T_s. The separation distance Z was normalized by Z_m, the position corresponding to the maximum value of α_i/N.

This position was obtained by numerically fitting a function of the form

$$\alpha(Z/Z_m)^2 \exp\left[-\beta(Z/Z_m)^2\right]$$

to the measured frequency distributions by the method of least squares. It is from this form of similar function that the mean value and standard deviation of apparent wavelength were finally determined, as follows.

We define now an average wavelength

$$\lambda = Z_m \int_0^\infty \frac{Z}{Z_m} P_{(\max)}\left(\frac{Z}{Z_m}\right) d\left(\frac{Z}{Z_m}\right),$$

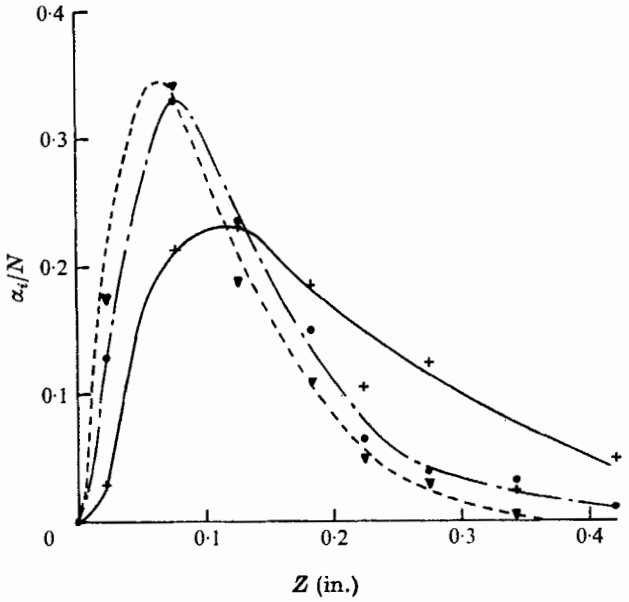

(*a*) Minimum

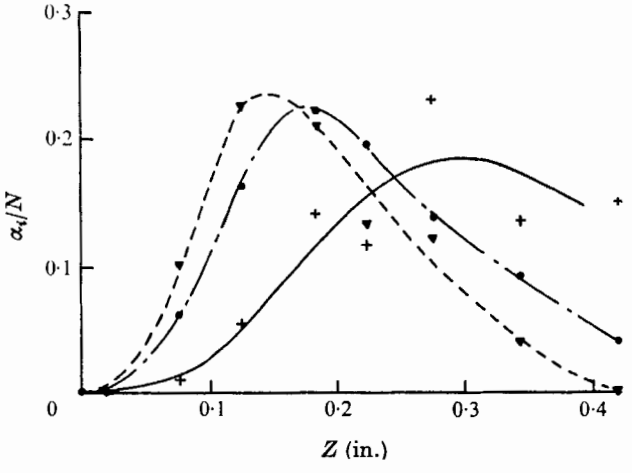

(*b*) Maximum

FIGURE 12. Typical frequency polygons at three velocities. +, U_0 = 11·3 ft/sec, T_s = 8 msec; ●, U_0 = 18·8 ft/sec, T_s = 1·5 msec; ▽, U_0 = 28·0 ft/sec, T_s = 0·625 msec.

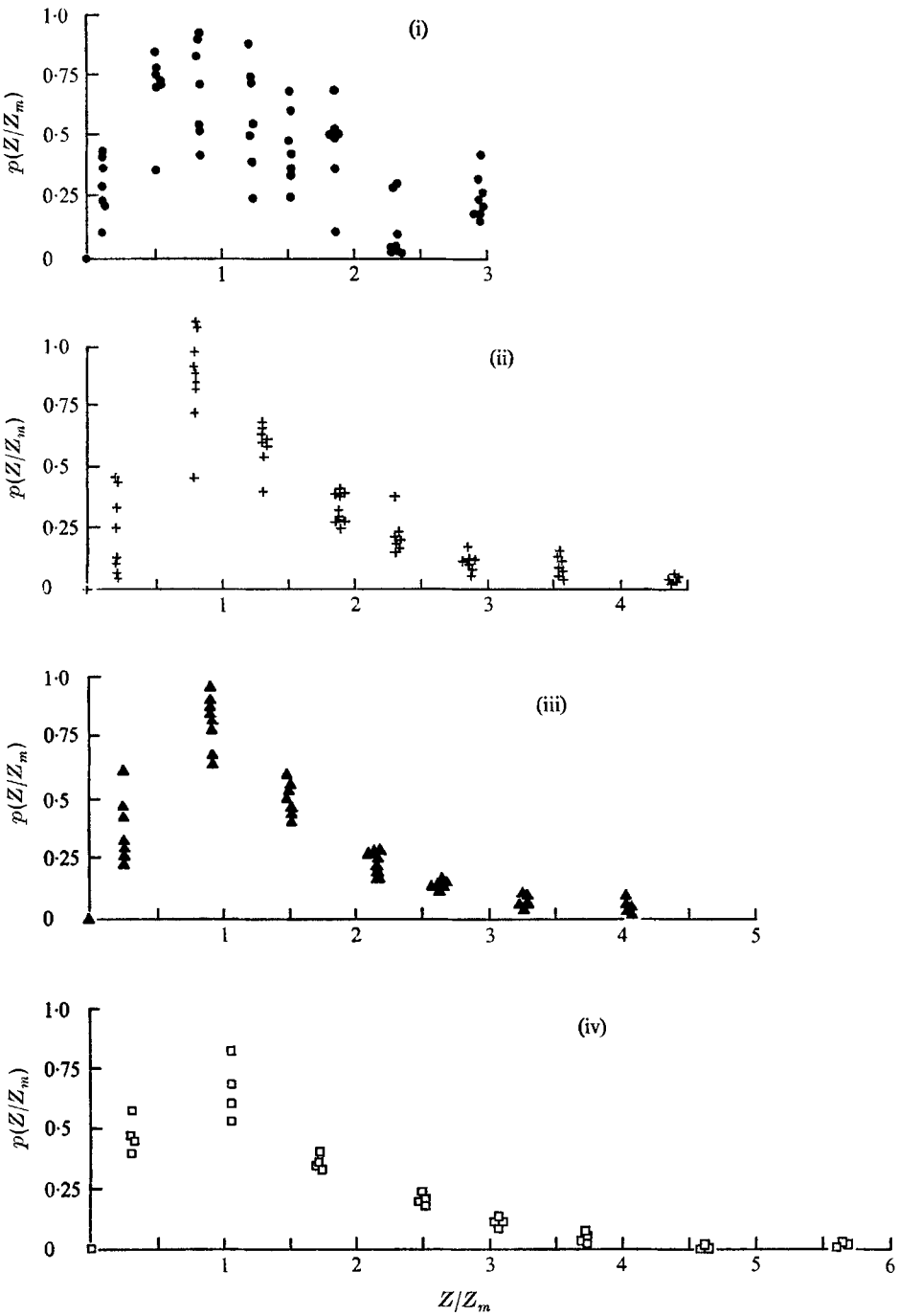

(*a*) Minimum

	(i)	(ii)	(iii)	(iv)
R_θ ($\simeq$)	2200	3300	4700	6500
U_0 (ft/sec)	11·3	18·8	28	39·5

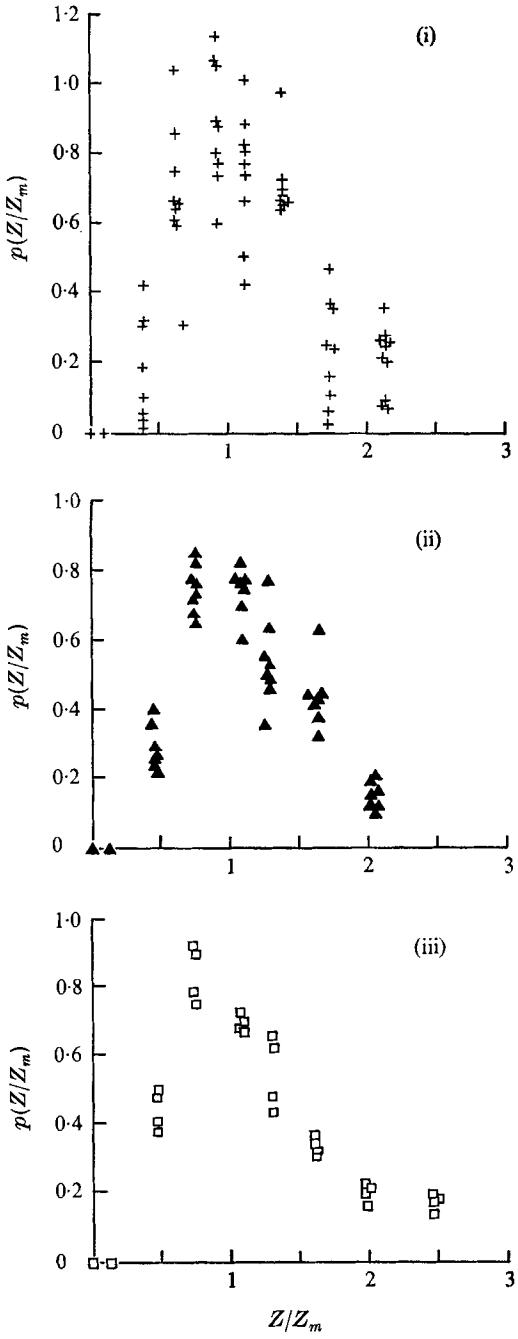

(*b*) Maximum

	(i)	(ii)	(iii)
R_θ ($\simeq$)	3300	4700	6500
U_0 (ft/sec)	18·8	28	39·5

FIGURE 13. Frequency polygons for four Reynolds numbers plotted in the normalized variable Z/Z_m. ●, $R_\theta \simeq 2200$; +, $R_\theta \simeq 3300$; △, $R_\theta \simeq 4700$; □, $R_\theta \simeq 6500$.

where $P_{\max}(Z/Z_m)$ is the probability that a maximum occurs in the interval Z/Z_m to $Z/Z_m + d(Z/Z_m)$, also,

$$\int_0^\infty P_{\max}\left(\frac{Z}{Z_m}\right) d\left(\frac{Z}{Z_m}\right) = 1.$$

A similar definition can be made for $\frac{1}{2}\lambda$ using the measurements for the minima locations.

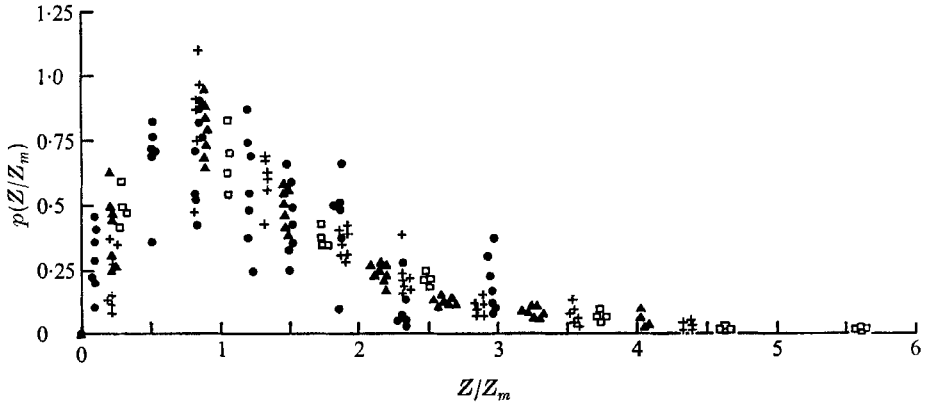

(*a*) Minimum

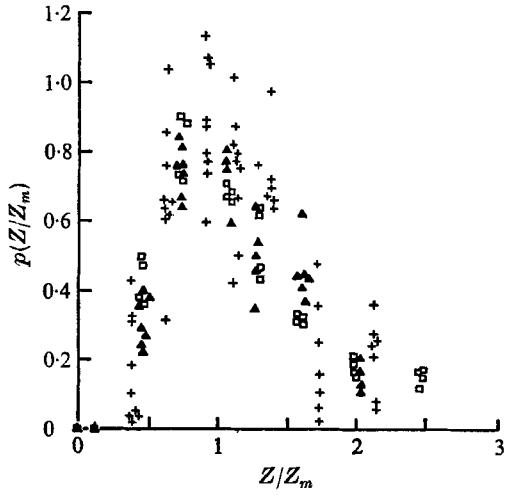

(*b*) Maximum

FIGURE 14. Composite plots of frequency polygons for four Reynolds numbers. ●, $R_\theta \simeq 2200$; +, $R_\theta \simeq 3300$; ▲, $R_\theta \simeq 4700$; □, $R_\theta \simeq 6500$.

It is clear from figure 13 that the measurements cannot determine the probability function completely for all Reynolds numbers. However they indicate that within the experimental scatter the shape of the distributions are similar. This becomes apparent when the data of figure 13 are replotted on two composite plots for maxima and minima, as shown in figure 14. On the basis of this observation the above integrals have been evaluated only for cases in which the experiments

provide full information about the probability distribution. Accordingly it was found that

$$\lambda = 1{\cdot}15\, Z_{m(\max)} \quad \text{for the maximum,}$$

$$\tfrac{1}{2}\lambda = 1{\cdot}125\, Z_{m(\min)} \quad \text{for the minimum.}$$

With this result the wavelengths were calculated for various Reynolds numbers and listed in table 1. The table also shows the variation of the non-dimensional wavelength $\lambda u^*/\nu$ and λ/δ with Reynolds number.

R_θ	u^* ft/sec	δ in.	$Z_{m(\max)}$ in.	$\dfrac{\lambda u^*}{\nu}$	$\dfrac{\lambda}{\delta}$	$Z_{m(\min)}$ in.	$\dfrac{\lambda u^*}{2\nu}$	$\dfrac{\lambda}{2\delta}$
2200	0·46	3·59	0·35	97·5	0·112	0·15	40·8	0·047
3300	0·74	3·24	0·20	89·0	0·071	0·10	43·7	0·035
4700	1·075	3·0	0·17	109·7	0·065	0·085	53·4	0·032
6500	1·48	2·8	0·17	151·2	0·070	0·075	65·2	0·030

TABLE 1

It is seen that the wavelength λ scales fairly consistently with the sublayer length parameter ν/u^* for the three lowest Reynolds numbers and has a value of

$$\lambda \simeq 100\nu/u^*,$$

a result consistent with Kline *et al.* (1967) and with the estimated value of Bakewell & Lumley (1967).

At $R_\theta = 6500$ the non-dimensional location of the third wire (the minimum resolvable location of the first maximum) was 60. Thus all occurrences of maximum in the range $0 < Z_{\max} u^*/\nu < 60$ were located at $\bar{Z}_{\max} u^*/\nu = 60$. This biases the probability density towards higher indicated wavelengths, as verified by the measurements.

5. Concluding remarks

The correlation coefficients $\hat{R}_{uu}$ shown in figures 7 and 8 give strong support to the concept that a fairly coherent structure exists in the sublayer. Instantaneous velocity distributions in the lateral (z) direction show local 'peaks' and 'valleys' that remind one of similar results observed by Klebanoff, Tidstrom & Sargent (1962) in connexion with their studies of laminar boundary-layer instability. The mean distance between these peaks is found to be equal approximately to 10 sublayer thicknesses obtained from the velocity correlation measurements. It should be mentioned that the standard deviation of this wavelength is rather large ($\sigma/\lambda \simeq 0{\cdot}4$), nevertheless, its coherence over its lifetime is surprisingly high.

The lifetime, incidentally, may be estimated on the basis of the maximum averaging time that gives consistent values for the wavelength. This is found to be relatively short, of the order of $0{\cdot}5\,\delta/U_0$ for the Reynolds number range under investigation. Unfortunately, this range is not large enough to indicate whether the time in fact scales with ν/u^{*2} or δ/U_0.

The results obtained so far raise a number of questions. The most relevant one has to do with the generation mechanism of the observed structure. Clearly it is much too early to speculate about this, and the next set of experiments will, in fact, be directed to deal with this problem. They will be designed under the assumption that the structure is the result of a sublayer instability mechanism produced by a locally superimposed pressure field. Whether or not such a conjecture is valid will have to be decided subsequently.

This research was supported under the National Science Foundation Grants GK 4004 and GK 24578.

REFERENCES

BAKEWELL, H. P. & LUMLEY, J. L. 1967 *Phys. Fluids*, **10** 1880.

CLAUSER, F. H. 1956 *Advances in Applied Mechanics*, vol. IV. Academic.

COLLIS, D. C. & WILLIAMS, M. J. 1959 *J. Fluid Mech.* **6**, 357.

CORINO, E. R. & BRODKEY, R. S. 1969 *J. Fluid Mech.* **37**, 1.

CORRSIN, S. 1947 *Rev. Scientific Instruments*, **18**, 469.

CORRSIN, S. 1957 *Some Current Problems in Turbulent Shear Flows*, p. 515. Naval Hydrodynamics Publication.

GRASS, A. J. 1971 *J. Fluid Mech.* **50**, 233.

KAPLAN, R. E. & LAUFER, J. 1969 *Proc. Twelfth Int. Cong. Appl. Mech.* p. 236. Standford University: Springer.

KIM, H. T., KLINE, S. J. & REYNOLDS, W. C. 1971 *J. Fluid Mech.* **50**, 133.

KLEBANOFF, P. S., TIDSTROM, K. D. & SARGENT, L. M. 1962 *J. Fluid Mech.* **12**, 1.

KLINE, S. J. & RUNSTADLER, P. W. 1959 *J. Appl. Mech.* **26***E*, p. 166.

KLINE, S. J., REYNOLDS, W. C., SCHRAUB, F. A. & RUNSTADLER, P. W. 1967 *J. Fluid Mech.* **30**, 741.

RAO, K. N., NARASIMHA, BADRI NARAYANAN, M. A. B. R. 1971 *J. Fluid Mech.* **48**, 339.

TOWNSEND, A. A. 1956 *The Structure of Turbulent Shear Flow*. Cambridge University Press.

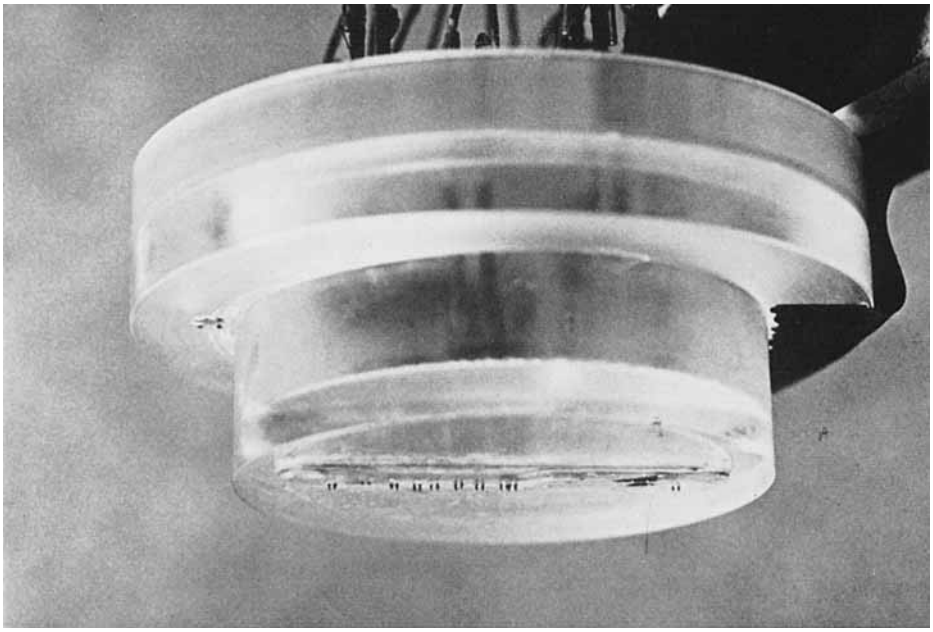

FIGURE 3. u plug probe.